Electrical and Mechanical Behaviors of Carbon Nanotube-Filled Polymer Blends

Man Wu, Leon Shaw

Department of Materials Science and Engineering, Institute of Materials Science, University of Connecticut, Storrs, Connecticut 06269

Received 14 March 2005; accepted 16 May 2005
DOI 10.1002/app.22255
Published online in Wiley InterScience (www.interscience.wiley.com).

ABSTRACT: Four carbon nanotube (CNT)-filled polymer blends, *i.e.*, CNT-filled polyethylene terephthalate (PET)/polyvinylidene fluoride, PET/nylon 6,6, PET/polypropylene, and PET/high-density polyethylene blends, have been injection-molded and characterized in terms of their microstructures, electrical conductivities, and mechanical properties. The distribution of CNTs in the polymer blends has been examined based on their wetting coefficients and minimization of the interfacial energy. The electrical conductivity and mechanical properties have been related to the cocontinuous polymer blends, the conductive path formed by CNTs, the CNT distribution, and the intrinsic properties of the constituent polymers. It is found that to obtain a CNT-filled polymer composite with both high electrical conductivity and good mechanical properties, it is preferred that most CNTs distribute in one polymer phase, while the other polymer phase(s) remain neat. © 2005 Wiley Periodicals, Inc. J Appl Polym Sci 99: 477–488, 2006

Key words: composites; blends; conducting polymers; mechanical properties; bipolar plates of PEM fuel cells

INTRODUCTION

Polymer electrolyte membrane fuel cells (PEMFCs), as an alternative power source, must be assembled into a fuel cell stack to get sufficient power for various applications. To achieve a significant improvement in the power density and a cost reduction by ~10 times for the automotive application of PEMFCs,[1] bipolar plates has been the subject of intensive research for the last decade. To date, graphite or carbon-based bipolar plates,[2,3] metal-based bipolar plates,[4–7] and polymer composite bipolar plates[8–11] have all been investigated. Suffered from its brittleness, the graphite bipolar plates not only need to have a thickness of several millimeters, but also have a high machining cost.[1,3] For metal-based bipolar plates, the corrosion of the plates in the fuel cell environment leads to a release of cations, which can result in an increase in membrane resistance as well as poisoning of the electrode catalysts.[4–7] Carbon-based polymer composite bipolar plates, in contrast, have the advantage of low costs, low weight, good chemical stability, and easy manufacturing. However, to obtain electrical conductivities high enough for the intended applications, high carbon concentrations (typically >50 vol %) are needed in the composite.[9–11] The conductive network in the composite is explained in terms of the percolation theory.[12] When the concentration of the conductive filler reaches a critical value, termed as the percolation threshold, the electrical conductivity will increase by several orders of magnitude.[12] After that, the increase in the conductivity becomes slow with further increasing in the filler concentration. In addition, it is well-known that the tensile strength of polymer composites decreases markedly if the filler concentration is too high.[13–15] That is, the high conductive materials are obtained at the expense of the desirable mechanical properties. Furthermore, when the filler concentration is high, manufacturing of composite bipolar plates also becomes more costly because injection-molding, which is suitable for mass manufacturing,[1] becomes difficult to use. Instead, compression molding, a relatively slow process, often becomes the choice of the processing method.[9,10]

To address the issue of the concurrent reduction in mechanical properties when a high filler concentration is used, making carbon nanotube (CNT)-filled polymer blends containing a triple-continuous structure in 3D space has been pursued recently.[16–18] The efficacy of this engineered-microstructure approach is demonstrated using a CNT-filled polyethylene terephthalate (PET)/polyvinylidene fluoride (PVDF) blend. In this CNT-filled polymer blend, the wetting coefficient is such that CNTs are preferentially located in the PET phase, while the PVDF phase contains almost no CNTs. As a result of such preferential distribution of

Correspondence to: L. Shaw.
U.S. Army through the Connecticut Global Fuel Cell Center; contract grant number: DAAB07–03-3-K415.

CNTs, the CNT-filledPET/PVDF blend exhibits 2500% improvement in electrical conductivity, 36% increase in tensile strength, and 320% improvement in elongation over the CNT-filled PET with the same carbon loading.[17,18] Thus, the triple continuous, carbon-filled polymer blends have great potentials for manufacturing conductive polymers with superior conductivity and strength for bipolar plate applications of PEM fuel cells. The underlying principle for the simultaneously improved electrical conductivity and mechanical properties observed in the CNT-filled PET/PVDF blend has been identified to be related to the formation of the triple-continuous structure in the CNT-filled polymer blend.[18] The continuous PET phase filled with CNTs provides the composite an electrical short circuit, whereas the continuous PVDF phase free from CNTs offers crack bridging and crack deflection to improve mechanical properties of the composite.[18]

The concept of cocontinuous polymer blends with carbon black preferentially located in one of the continuous polymer phases or at the polymer-blend interface has been studied for more than a decade with an aim to reduce the percolation threshold. Examples of this kind are the work by Geuskens et al. in as early as 1987,[19] which shows that for the same carbon loading, the resistivity of the cocontinuous polymer/rubber blends is several orders of magnitude smaller than that of the single polymer/carbon black composites. Recent works on polymer/elastomer combinations[20,21] and on polymer/polymer systems[22–29] have also shown that the double percolation approach can produce conducting materials at a lower filler concentration. All of these studies suggest that polymer blends can be an interesting approach for making conductive polymers. However, all the work cited above is limited to low carbon concentration systems with the resistivity at 10^2 Ω cm or higher, which is much higher than the desired values (10^{-1} to 10^{-3} Ω cm) for the bipolar plate applications.

In this study, the concept of the triple-continuous structure is applied to several polymer/polymer blends loaded with CNTs, with the aim to obtain polymer-based composites with high enough electrical conductivities and sufficient mechanical properties for the bipolar plate application of PEM fuel cells. The results obtained are compared with those of the previous studies[17,18] in which the CNT-filled PET/PVDF system has been investigated. The distribution of CNTs in the polymer blends is examined in terms of their wetting coefficients and minimization of the interfacial energy. The relationships among the microstructure, electrical conductivity, and mechanical properties are studied with an emphasis on achieving the simultaneous improvement in both conductivity and tensile strength.

EXPERIMENTAL

Four polymer blends were used as the matrix for conductive CNTs. Each polymer blend system was composed of two kinds of immiscible polymers. They were (i) polyethylene terephthalate (PET)/polyvinylidene fluoride (PVDF), (ii) PET/polypropylene (PP), (iii) PET/high-density polyethylene (HDPE), and (iv) PET/nylon 6,6.

Two types of PET were used in this study; one was neat PET and the other the CNT-filled PET. The latter was obtained from Hyperion Catalysis International, Inc. and prefilled with 15 wt % (i.e., 12 vol %) CNTs through a twin-screw extruder. The CNT-filled PET came in a cylindrical pellet form with sizes of 3 mm in diameter and 2.5 mm in height. The CNTs used to prepare master batches of the CNT-filled PET pellets were hollow, multi-walled tubes with 8–15 walls and a graphitic microstructure. The outside diameter of the tube was approximately 10–15 nm, whereas the inside diameter was about 5 nm. The tube had a very large aspect ratio with the tube length in the range of 10–15 μm.

The PVDF used in this study was Kynar® 720 pellets in a biconvex-lens shape with 5 mm in diameter and about 2 mm in thickness at the center of the lens, obtained from Atofina Chemicals, Inc. The nylon 6,6 was Celanese Nylon 6/6® 1000–1 pellets in a cylindrical shape with sizes of 2 mm in diameter and 2.5 mm in height, while the PP and HDPE pellets came in the similar shape and size to that of PVDF.

Each CNT-filled polymer blend was prepared in the same way. First, the CNT-filled PET was dried at 150°C for 5 h, and the second polymer was dried at 100°C for 1 h. The dried CNT-filled PET and second polymer pellets were then mixed in a 1 to 1 volume ratio, using a rotating bottle for 5 min. As a result of this ratio, the CNT concentration in each composite system was 6.0 vol %. Final composite samples were prepared using an injection-molding machine (Arburg 221–75-350). Two types of injection-molded samples were fabricated, as shown in Figure 1, with one for electrical conductivity measurements and the other for mechanical testing. The process parameters of the injection-molding were summarized in Table I. The processing conditions were determined based on the melting points and thermal decomposition temperatures of the polymers in each polymer blend. Differential scanning calorimetry (DSC) and thermogravimetric analysis (TGA) were utilized to establish the melting and thermal decomposition temperatures of all the polymers used in this study. In all these simultaneous DSC/TGA analyses, a heating rate of 10°C/min was employed using a TA instrument (SDT 2960 Simultaneous DTA/TGA) under a flowing argon atmosphere from ambient temperature to 400°C.

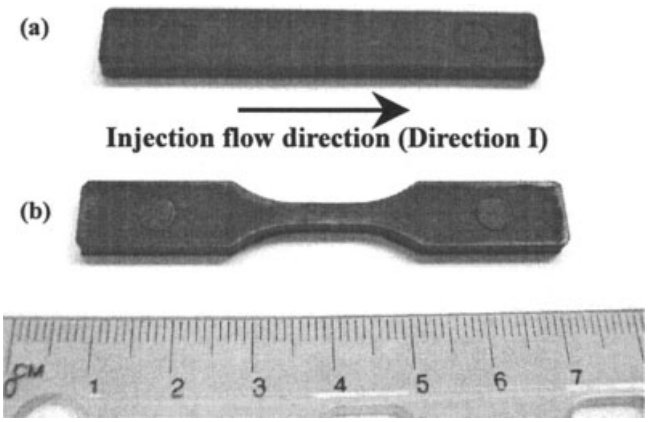

Figure 1 Specimens obtained from injection-molding: (a) for conductivity measurements and (b) for tensile tests.

The microstructure of and the CNT distribution in polymer blends were observed with an environmental scanning electron microscope (Phillips ESEM 2020). The SEM samples were prepared in four different approaches, depending on the purpose of the observation. The first approach entailed fracturing specimens in liquid nitrogen to reveal the fracture surface for microstructural observations. The second sample preparation approach consisted of cutting the injection-molded samples with a diamond blade, followed by polishing with Al_2O_3 suspensions down to 0.05 μm, and then ion-etching using an Argon Ion Sputter Gun (Physical Electronic Industry, Inc.) with a 3kV voltage and a 45° angle of the sputter gun with respect to the fracture surface for 45 min to reveal the position of CNTs. This set of SEM samples allowed examination of the microstructure with minimum loading before the SEM observation. The third approach for SEM sample preparation was to cut the tension-tested samples, followed by polishing and ion etching with the same process parameters as the second approach to reveal the crack initiation and propagation patterns on the cross section parallel to the tensile loading axis. The last sample preparation approach was the direct observation of the fracture surface of the samples fractured under tensile loading at room temperature. This set of samples offered another perspective regarding deformation and fracture mechanisms under tensile loading. All the SEM samples were coated with gold-palladium before the SEM observation to avoid charging during the SEM observation.

Tensile specimens were in a dog-bone shape and had a gauge length of 10 mm (Fig. 1). The tensile test was conducted at a constant crosshead speed of 6 mm/min, using a servo-hydraulic loading frame. An extensometer was attached to the gauge length of the sample to provide the strain value as a function of loading.

To measure the electrical conductivity, a QuadTech 1880 Milliohmmeter was utilized to get the resistance for samples with a certain cross section area and thickness. Based on the resistance (R) recorded, the electrical conductivity was calculated as follows:

$$\sigma = \frac{d}{AR} \tag{1}$$

where d is the specimen thickness between the two electrodes and A is the cross-sectional area perpendicular to the current direction in the sample. Silver paste was used in all the measurements to ensure good contact of the sample surface with the electrodes. Furthermore, the electrical conductivity was measured in two directions for the injection-molded rectangular plates (Fig. 1); one was parallel to the major flow direction of injection-molding (called Direction I hereafter), and the other was perpendicular to Direction I (called Direction II).

RESULTS AND DISCUSSION

Injection molding of CNT-filled polymer blends

Figure 2 shows the simultaneous DSC and TGA traces of neat PET and nylon 6,6 ranging from ambient temperature to 400°C determined under a flowing argon atmosphere. Based on the endothermic peaks the melting temperatures, T_m, of neat PET and nylon 6,6 are determined to be 247 and 263°C, respectively. If the temperature at which weight loss reaches 0.5% is defined as the thermal decomposition temperature

TABLE I
Processing Parameters in Injection-Molding

	Nozzle temp. (°C)	Barrel temp. (°C)			Mold temp. (°C)	Screw speed (rpm)	Injection speed (mm/s)
		Pumping section	Melting section	Feeding section			
CNT-filled PET/PVDF	285	275	270	265	Ambient	200	80
CNT-filled PET/PP	270	265	260	255	Ambient	200	80
CNT-filled PET/HDPE	260	255	245	240	Ambient	200	80
CNT-filled PET/nylon 6,6	275	268	260	250	Ambient	200	80
CNT-filled PET/PET	280	270	265	260	Ambient	200	80

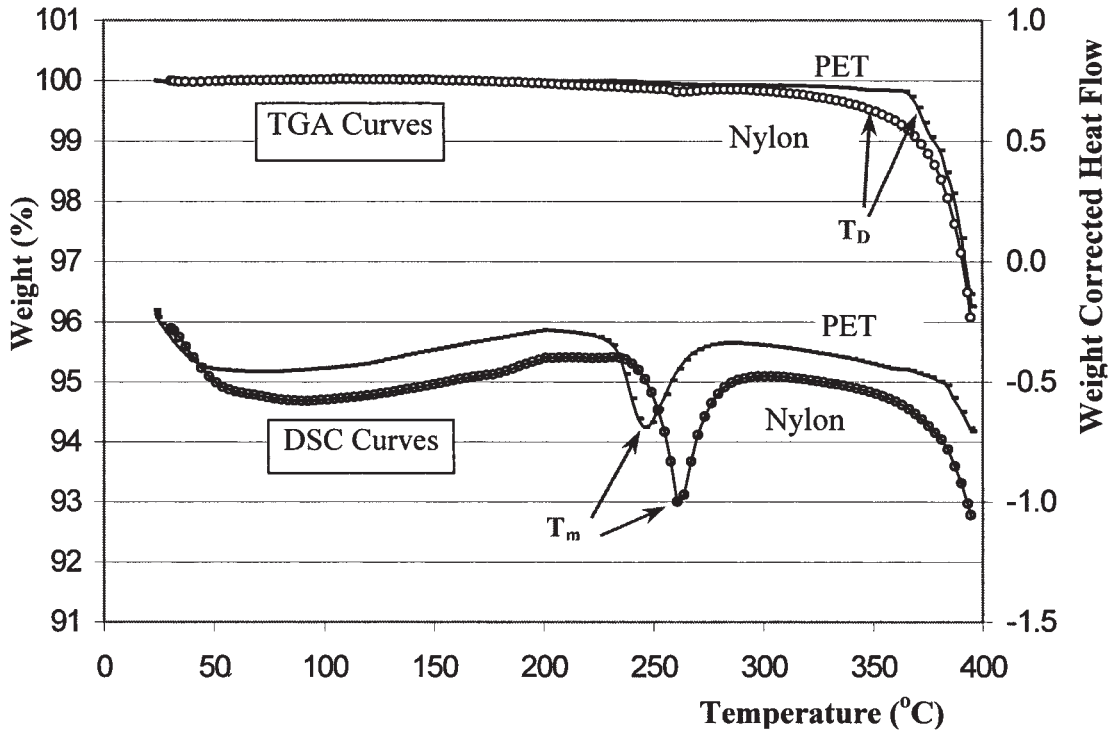

Figure 2 Simultaneous DSC and TGA traces of neat PET and nylon 6,6 determined with a heating rate of 10°C/min under a flowing argon atmosphere.

under a flowing argon atmosphere, then the thermal decomposition temperatures, T_D, are 372 and 350°C for neat PET and nylon 6,6, respectively. The processing temperature for injection-molding has to be higher than the melting temperatures of the neat polymers used in the polymer blend, and furthermore is preferably lower than the decomposition temperatures defined by 0.5% weight loss to avoid noticeable degradation of polymer blends.

Table II summarizes all the T_m and T_D measured for all the polymers used in this study. Comparisons between Tables I and II indicate that the nozzle temperature for injection-molding has been selected to be between T_m and T_D for CNT-filled PET/PET, PET/PVDF, and PET/nylon 6,6 blends. In contrast, the nozzle temperature for CNT-filled PET/PP and PET/HDPE blends has been selected to be slightly higher than the decomposition temperatures of neat PP and HDPE. Such selections in the nozzle temperatures slightly higher than the decomposition temperatures of neat PP and HDPE are due to the small gap between the decomposition temperatures of PP (262°C) and HDPE (255°C) and the melting temperature of PET (247°C), and implemented to ensure the injection moldability at the slight expense of decomposition.

TABLE II
Thermal Analysis Data of Neat Polymers

Materials	T_m (°C)	T_D (°C)
PET	247	372
PVDF	176	386
HDPE	133	255
PP	148	262
Nylon 6,6	263	350

T_m and T_D represent the melting temperature and thermal decomposition temperature, respectively.

Composite microstructures

Figure 3 shows the fracture surfaces of CNT-filled PET/PVDF, PET/PP, and PET/HDPE blends fractured at the liquid nitrogen temperature. It is noted that there are two distinct regions in each polymer blend: one contains CNTs (region A) and the other does not (region B). To estimate the area fractions of regions A and B in each polymer blend, 100 SEM images randomly selected at a magnification of 10,000× have been examined for each polymer blend. The average area fraction of region A counted from these 100 images is found to be 53, 57, and 57% for CNT-filled PET/PVDF, PET/PP, and PET/HDPE, respectively. Recall that these CNT-filled polymer blends are fabricated via mixing 50 vol % of the CNT-filled PET with 50 vol % of the second polymer (i.e., PVDF, PP, or HDPE). Thus, these data indicate that a small amount of CNTs has transferred to the second polymer phase during the injection-molding process.

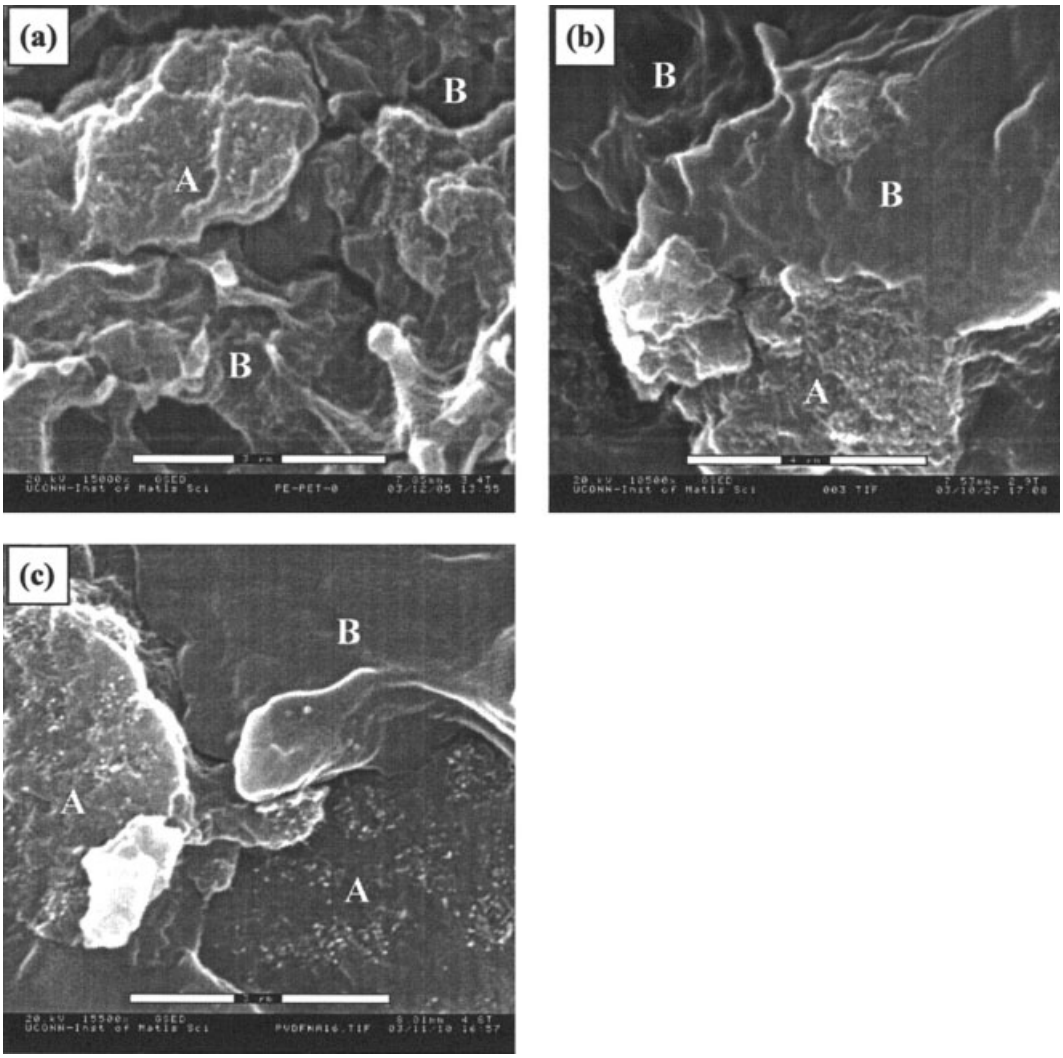

Figure 3 ESEM images of the fracture surface of (a) CNT-filled PET/HDPE, (b) CNT-filled PET/PP, and (c) CNT-filled PET/PVDF polymer blends fractured at the liquid nitrogen temperature. Region A contains CNTs, whereas region B is free from CNTs.

Furthermore, there is more CNT transfer in the CNT-filled PET/PP and PET/HDPE systems than that in the CNT-filled PET/PVDF system. Such a CNT transfer phenomenon is believed to be related to two mechanisms; one is the CNT transfer forced mechanically due to the shearing action derived from the screw rotation during the mixing stage of the injection-molding process, and the other is the CNT transfer driven by the thermodynamic driving force to minimize the interfacial energy of the CNT-filled polymer blend. It is argued that the former mechanism plays a key role in the CNT transfer for the CNT-filled PET/PVDF system, whereas both mechanisms are operational in the CNT transfer for CNT-filled PET/PP and PET/HDPE systems. This viewpoint is supported by the thermodynamic analysis detailed below.

For a polymer blend, the distribution of carbon particles (or nanotubes) can be predicted by the state of the minimum interfacial energy if the equilibrium state is reached. Such a minimum interfacial energy state can be determined by Young's equation[30]

$$\omega_a = \frac{\gamma_{C-B} - \gamma_{C-A}}{\gamma_{A-B}} \tag{2}$$

where ω_a is the wetting coefficient and γ_{C-A}, γ_{C-B}, and γ_{A-B} are the interfacial energy between carbon and polymer A, carbon and polymer B, and polymers A and B, respectively. When $\omega_a > 1$, carbon particles preferentially distribute within polymer A. When $-1 < \omega_a < 1$, carbon particles distribute at the interface of the polymer blend. Finally, when $\omega_a < -1$, carbon particles distribute within polymer B. The interfacial energy between two phases, γ_{12} (for phases 1 and 2), in eq. (2) can be estimated using the harmonic-mean equation[31]

$$\gamma_{12} = \gamma_1 + \gamma_2 - 4\left[\frac{\gamma_1^d \gamma_2^d}{\gamma_1^d + \gamma_2^d} + \frac{\gamma_1^p \gamma_2^p}{\gamma_1^p + \gamma_2^p}\right] \tag{3}$$

TABLE III
The ω_a Value and the Predicted CNT Location for Four CNT-Filled Polymer Blends

Materials	Wetting coeff. (ω_a)	Predicted location of CNTs in the composite
CNT-filled PET/PVDF	5.10	PET
CNT-filled PET/PP	0.98	Interface
CNT-filled PET/HDPE	0.05	Interface
CNT-filled PET/nylon 6,6	3.33	PET

where γ stands for the surface tension and subscripts 1 and 2 refer to phases 1 and 2, respectively. Further, $\gamma = \gamma^d + \gamma^p$, γ^d is the dispersion component of surface tension, and γ^p is the polar component.

Based on the surface tension data of carbon, PET, PVDF, PP, HDPE, and nylon 6,6, as well as their dispersion and polar components at 180°C,[31] the ω_a values for all the CNT-filled polymer blends investigated in this study are calculated and listed in Table III. As shown in the table, there are two different situations for CNT distribution in these immiscible polymer blends. For CNT-filled PET/PVDF and PET/nylon 6,6 blends, the consideration of the interfacial energy alone predicts that CNTs should stay in the PET phase. In contrast, the predicted location for CNTs in the CNT-filled PET/PP and PET/HDPE blends is at the interface between the PET phase and the second polymer phase. Thus, these is a thermodynamic driving force for CNTs to transfer from the PET phase to the interface for the CNT-filled PET/PP and PET/HDPE systems, while this is not the case for the CNT-filled PET/PVDF and PET/nylon 6,6 systems. It is this difference that has resulted in more CNT transfer into the second polymer phase in the CNT-filled PET/PP and PET/HDPE than that in the CNT-filled PET/PVDF. Furthermore, the thermodynamic analysis performed earlier also suggests that a small amount of the CNT transfer into the second polymer phase in the CNT-filled PET/PVDF blend, as evidenced by the increase of the CNT-filled region from 50 to 53 vol %, is not driven by the thermodynamic driving force, but due to the shearing action derived from the screw rotation during the mixing stage of the injection-molding process.

To evaluate the area fractions of the CNT-filled region (region A) and CNT-free region (region B) in the CNT-filled PET/nylon 6,6 blend, the injection-molded samples were cut with a diamond blade, polished using Al_2O_3 suspensions down to 0.05 μm, ion etched using an argon ion sputter gun, and then coated with gold-palladium. The cross sections so prepared are shown in Figure 4. It is obvious that the microstructure of the CNT-filled PET/nylon 6,6 is quite different from that of the CNT-filled PET/PVDF, PET/PP, and PET/HDPE. First, large nylon regions free from CNTs at millimeter scales (region C marked in Fig. 4) are present. Second, there are microcracks at the interface between the large nylon region and the CNT/PET/nylon-mixed region (regions A + B in Fig. 4). Third, the CNT/PET/nylon-mixed region is mainly composed of the CNT-filled PET (region A) and CNT-free nylon phase (region B). Fourth, the area fraction of

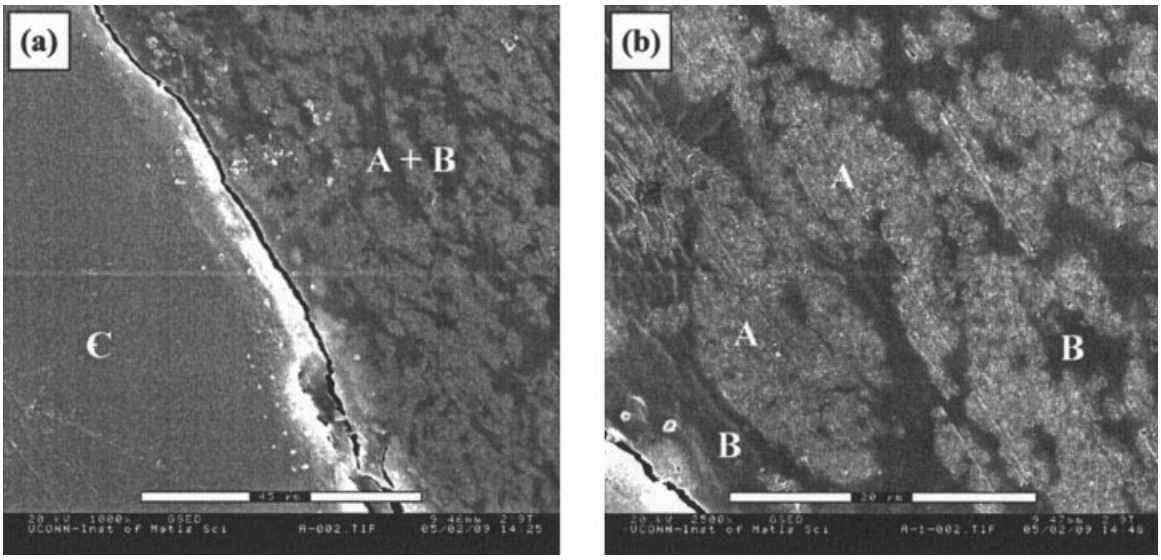

Figure 4 SEM images of the cross sections of the CNT-filled PET/nylon 6,6 blend prepared by cutting with a diamond blade, polishing with Al_2O_3 suspensions, ion etching with an argon ion sputter gun, and finally coating with gold-palladium. Region A contains CNTs, whereas regions B and C are free from CNTs. (a) A low magnification image showing the presence of a large nylon region (marked as C) and a microcrack at the interface between regions C and (A + B), and (b) a high magnification image of the (A + B) region in (a).

TABLE IV
Coefficients of Thermal Expansion (CTE) for the Polymers Used in the CNT-Filled Polymer Blends [32]

Materials	Temperature range (°C)	Coefficient of thermal expansion (10^{-6}/K)
PET	−40 to 150	20–80
PVDF	−40 to 150	80–140
PP	−30 to 100	100–180
HDPE	25 to 100	100–200
Nylon 6,6	−30 to 150	90

region A is found to be about 53%, while the area fraction of the CNT-free regions (i.e., regions B + C) is about 47%.

The markedly different microstructure obtained in the CNT-filled PET/nylon 6,6 blend is attributed to the insufficient breakdown and mixing during the injection-molding process. Recall that for CNT-filled PET/PVDF, PET/PP, and PET/HDPE blends, the size of the neat polymer region (i.e., region A) is typically in the range of 1–40 μm^2 (Fig. 3), which is substantially smaller than the original sizes of the cross sections (several millimeters) of the PVDF, PP, and HDPE pellets. In contrast, the large neat nylon regions found in the CNT-filled PET/nylon 6,6 blend have the sizes similar to the original size of nylon 6,6 pellets. This insufficient breakdown of nylon 6,6 regions and lack of uniform mixing is more likely related to the relatively low processing temperatures used in the injection-molding process, as shown in Table I. It can be seen that the difference between the processing temperatures (275°C at the nozzle and 268°C at the pumping section) and the melting temperature of nylon 6,6 (263°C) is smaller than 15°C. The small overheating results in high viscosities of the nylon 6,6 melt and makes the mixing difficult during the injection-molding process. As a result, some nylon 6,6 molten regions are fully broken up and mixed with the CNT-filled PET phase, whereas some do not in the melting and pumping sections during the injection-molding process.

The presence of microcracks at the interface between the large neat nylon region and the CNT/PET/nylon-mixed region suggest that the formation of microcracks is related to the presence of large nylon regions. It is proposed that the underlying mechanism for the formation of microcracks is the mismatch in the coefficient of thermal expansion (CTE) between PET and nylon. Table IV lists the CTEs for all the polymers investigated in this study.[32] Note that all of the polymers used in this study have higher CTEs than PET; therefore, residual thermal stresses are present in all of the CNT-filled polymer blends investigated here. However, when the neat polymer region (region A) and CNT-filled PET region (region B) are mixed at micrometer scales, the residual thermal stresses are small, and no microcracks are generated during the cooling process. In contrast, when the neat polymer region is large (in millimeter scales as in the case of large nylon regions), the residual thermal stresses become large and lead to the formation of microcracks at the interface between the large nylon region and the CNT/PET/nylon-mixed region.

The finding that the area fraction of the CNT-filled region in the CNT-filled PET/nylon 6,6 is about 53% is consistent with the interfacial energy consideration performed earlier, and suggests that the small amount of CNT transfer to the nylon phase is mainly caused by the shearing action derived from the screw rotation during the injection-molding process.

Electrical conductivities of CNT-filled polymer blends

The electrical conductivities of injection-molded, CNT-filled polymer blends have been measured and are summarized in Table V. For comparison, Table V also includes the literature value of electrical conductivities of neat polymers used in this study. For each polymer blend, electrical conductivities are measured in two directions to see whether the specimen is isotropic or not. One direction is parallel to the major flow direction of the injection-molding process,

TABLE V
Electrical Conductivities of CNT-Filled Polymer Blends and Neat Polymers

Materials	Conductivity in direction I (S/cm)	Conductivity in direction II (S/cm)	Ratio of conductivity in direction I to direction II
CNT-filled PET/PVDF	0.059	0.0114	5.2
CNT-filled PET/PP	0.021	0.0023	8.9
CNT-filled PET/HDPE	0.011	0.0014	7.7
CNT-filled PET/nylon 6,6	0.011	0.0005	23.4
PET[32]	>1.0E-14	N/A	N/A
PVDF[34]	1.0E-13	N/A	N/A
HDPE[12]	1.0E-19	N/A	N/A
PP[12]	1.0E-19	N/A	N/A
Nylon 6,6[12]	1.0E-15	N/A	N/A

termed as Direction I hereafter (see Fig. 1), and the other is perpendicular to the major flow direction of the injection-molding process (called as Direction II). It is found that there is large difference in conductivity between these two directions. For CNT-filled PET/PVDF, PET/PP, and PET/HDPE, the conductivity in Direction I is about 4–8 times higher than that in Direction II. For CNT-filled PET/nylon 6,6, the conductivity difference in the two directions is even larger with Direction I having the conductivity >22 times higher than Direction II. The anisotropy found in all the specimens is most likely related to the partial alignment of CNTs in the polymer blend caused by the shear stress induced by the drag force of the die surface during injection flow.

It is also noticeable that even though all the polymer blends have the same CNT concentration of 6.0 vol %, different polymer blends display different conductivities. The highest conductivity obtained from the CNT-filled PET/PVDF in Direction I is 2.8–5.4 times of the highest conductivities obtained from other CNT-filled polymer blends in Direction I. The better conductivity obtained from the CNT-filled PET/PDVF blend in comparison with the CNT-filled PET/PP and PET/HDPE blends is attributed to its less CNT transfer to the second polymer phase. Such a reasoning is supported by the following analysis.

Given that all of the CNT-filled polymer blends in this study are prepared with 50 vol % of the CNT-filled PET phase (with 12 vol % CNTs) plus 50 vol % of the second immiscible polymer phase (with no CNTs), it is reasonable to assume that both the CNT-filled PET phase and the second immiscible neat polymer phase have formed self-continuous 3D networks in the polymer blends. This expectation is confirmed by the microstructure examination (see under Composite Microstructures), which reveals that the area fractions of the CNT-filled region and the CNT-free region are both near 50%. Furthermore, the electrical conductivity data suggests that the CNTs within the PET phase have also formed a 3D conductive path because the electrical conductivity has been increased from the neat polymers to the CNT-filled polymer blends by about 11–17 orders of magnitude. With such three self-continuous 3D structures, the conductive CNT-filled PET network and the nonconductive second polymer phase can be treated as parallel conductors, and the resulting resistivity, ρ, of the CNT-filled polymer blend can be estimated using the statistical percolation model proposed by Bueche[33]

$$\rho = \frac{\rho_c \rho_n}{V_n \rho_c + \omega(1 - V_n)\rho_n} \tag{4}$$

where ρ_c and ρ_n are the resistivities of the conductive and nonconductive phases, respectively; V_n is the volume fraction of the nonconductive phase, and ω is the fraction of the conductive phase being incorporated into the conducting network. The largest possible value for ω is 1, which corresponds to the case where all the CNT-filled PET regions are incorporated into the conductive network. For the present CNT-filled polymer blends, eq. (4) can be reduced to

$$\rho \approx \frac{\rho_c}{\omega(1 - V_n)} \tag{5}$$

because $\rho_n \gg \rho_c$. For example, ρ_n is 10^{13} Ω cm for PVDF[34] and ρ_c is only 4 Ω cm for the PET phase with 12 vol % CNTs.[18] Equation (5) can be utilized to qualitatively explain the electrical conductivity data obtained in this study. The CNT transfer from the PET phase to the second polymer phase will increase the resistivity of the CNT-filled PET, ρ_c, but at the same time will decrease the volume fraction of the nonconductive phase, V_n. However, the change in V_n is very small (e.g., from 50 to 43 vol % for the CNT-filled PET/PP and PET/HDPE blends). In contrast, the change in ρ_c can be potentially very large with changes of several orders of magnitude if the original concentration of CNTs in the PET phase is near the percolation threshold. The CNT transfer to the second polymer phase could also lead to a reduction in ω because the newly CNT-filled polymer regions may not be incorporated into the conductive network. Even when they are incorporated, their resistivities are unlikely to be as low as that of the CNT-filled PET regions because these newly CNT-filled polymer regions are most likely to have lower CNT concentrations than the CNT-filled PET regions. Therefore, based on the possible range of change for the parameters in eq. (5), it can be stated that the CNT transfer to the second polymer phase during the injection-molding process will, in general, increase the resistivity of the resulting composite, and thus is undesirable for improving the electrical conductivity. The present set of experiments backs this theoretical analysis, showing that the CNT-filled PET/PVDF has the highest electrical conductivity because it has the least CNT transfer to the second polymer phase.

Finally, it is noted that the CNT-filled PET/nylon 6,6 blend exhibits the lowest electrical conductivity among all the systems investigated. Although the CNT transfer to the second polymer phase for the CNT-filled PET/nylon 6,6 is small (*i.e.*, similar to the CNT-filled PET/PVDF blend), the presence of microcracks in this composite is believed to be responsible for the lowest electrical conductivity observed.

Mechanical properties of CNT-filled polymer blends

Figure 5 summarizes the tensile stress and elongation at break for all the CNT-filled polymer blends inves-

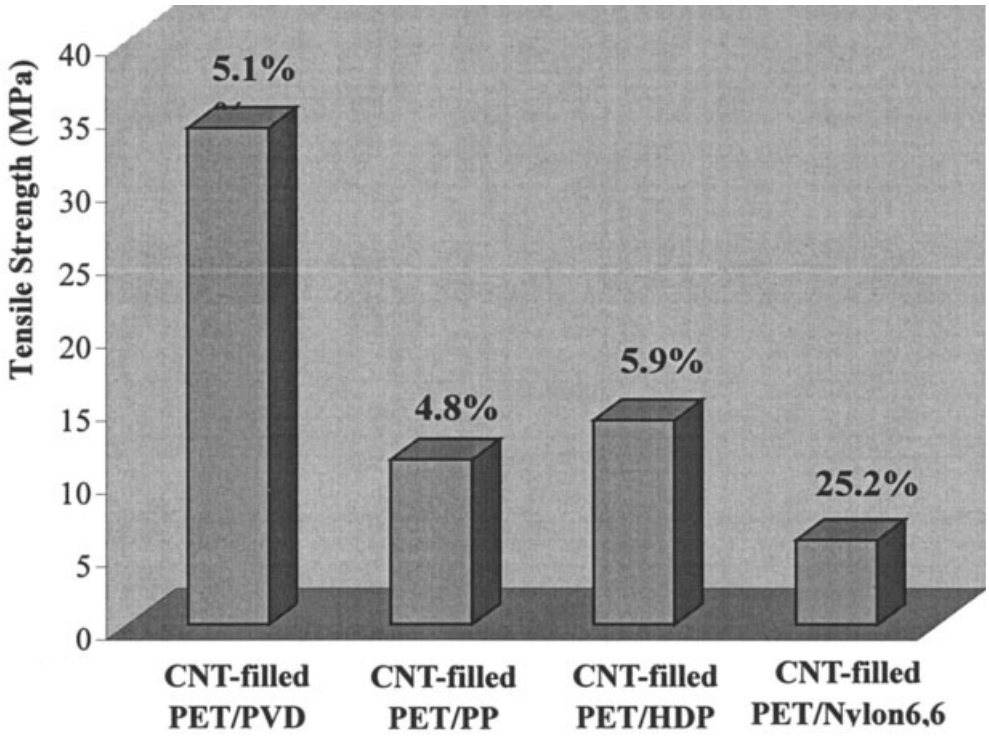

Figure 5 Tensile properties of CNT-filled polymer blends. The number shown on the top of the column is the corresponding elongation at break for each CNT-filled polymer blend.

tigated. Note that the CNT-filled PET/PVDF possesses the highest tensile stress at break, whereas the CNT-filled PET/nylon 6,6 exhibits the lowest tensile stress. The different mechanical properties exhibited by these CNT-filled polymer blends can be understood based on the key factors that dictate the mechanical properties of the CNT-filled polymer blends. These key factors include (i) the intrinsic properties of the constituent polymers, (ii) interfacial properties between the constituent polymers in the polymer blend, (iii) effects of CNTs on the properties of the polymers, (iv) the distribution of CNTs in the polymer blend, and (v) processing defects in the CNT-filled polymer blend.

Figure 6 lists the tensile stress and elongation at break for all the neat polymers measured in this study. If only the intrinsic properties of the constituent polymers are considered, PET/nylon 6,6 blends would offer the highest tensile stress at break. However, this is not observed. In fact, the CNT-filled PET/nylon 6,6 blend has the lowest tensile stress at break because of the presence of microcracks at the as-injection-molded condition. The next candidate that could offer the best tensile stress at break is the CNT-filled PET/PVDF blend. This has indeed been observed experimentally (Fig. 5). Thus, as expected, the intrinsic properties of the constituent polymers have played an important role in determining the final properties of the resulting CNT-filled polymer blends. In what follows, it will be shown that the effect of CNTs on the mechanical properties of the polymers and the distribution of CNTs within the polymer blend also impose strong influence on the final properties of the resulting CNT-filled polymer blends.

It has been shown in a previous study[18] that the addition of 6 vol % CNT into PET has resulted in reductions in both tensile stress (from 34 to 25 MPa) and elongation at break (from 2.2 to 1.2%). As such, the CNT-filled PET phase can be expected to have a very low elongation at break (only a few percent) in comparison with the neat polymer phase in the polymer blend (Fig. 6). Because of its low elongation at break, the CNT-filled PET region would fracture first under tensile loading. This is indeed confirmed by the SEM observation on the cross section of the CNT-filled PET/PVDF samples after tensile loading.[18] As shown in Figure 7, under tensile loading microcracks preferentially initiate and propagate within the CNT-filled PET phase. In contrast, the neat PVDF phase free from CNTs in the CNT-filled PET/PVDF blend has provided crack bridging and crack deflection to strengthen the CNT-filled polymer blend. As a result, the CNT-filled PET/PVDF blend has higher tensile stress and elongation at break than the CNT-filled PET with the same CNT loading.[18]

Similar crack bridging and fracture behavior are expected for the CNT-filled PET/PP and PET/HDPE blends because the neat PP and HDPE phases also

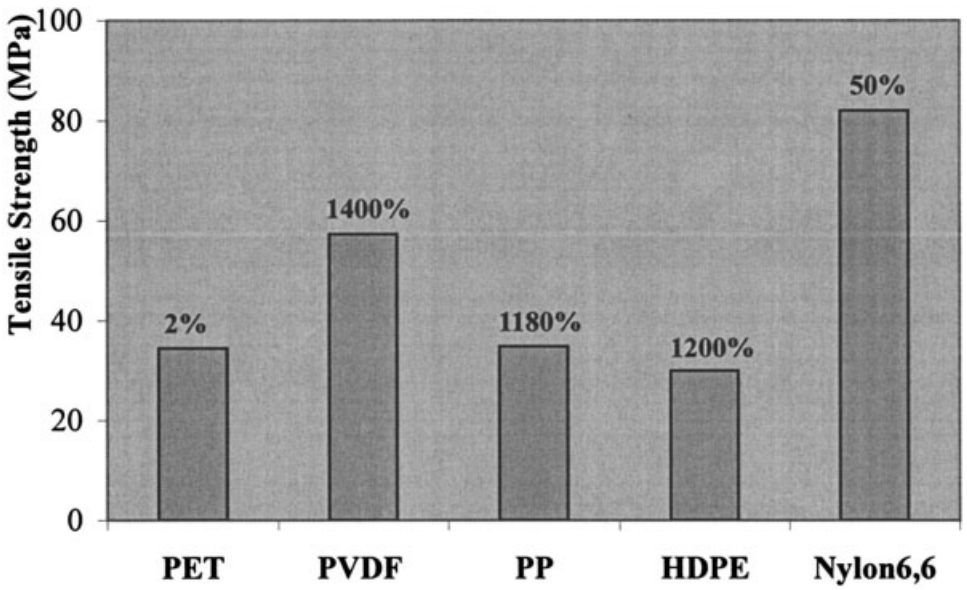

Figure 6 Tensile properties of neat polymers measured in this study. The number shown on the top of the column is the corresponding elongation at break for each neat polymer.

have the elongation at break substantially larger than that of the CNT-filled PET. This is indeed the case. Shown in Figure 8 are the fracture surfaces of the CNT-filled PET/PP and PET/HDPE blends after tensile fracture at room temperature. Note that although the fracture surface is perpendicular to the tensile loading axis, there are cracks parallel to the tensile loading axis (termed parallel cracks hereafter). Furthermore, these parallel cracks are mainly present at the interface between the CNT-filled PET and the neat polymer phase. Such parallel cracks are indicative of crack bridging and deflection mechanisms; these parallel cracks are generated because of the difference in the transverse shrinkage between the CNT-filled PET and the neat polymer phase. As discussed previously, microcracks perpendicular to the tensile loading axis will form in the CNT-filled PET region first because of its low elongation at break, and the subsequent tensile load will be mainly carried by the bridging ligaments of the neat polymer phase. Once the perpendicular microcracks are formed, the CNT-filled PET region will cease to shrink transversely, while the neat polymer phase continues to stretch longitudinally and shrink transversely. The difference in the transverse shrinkage creates the tensile stress in the transverse direction and leads to the formation of parallel cracks.

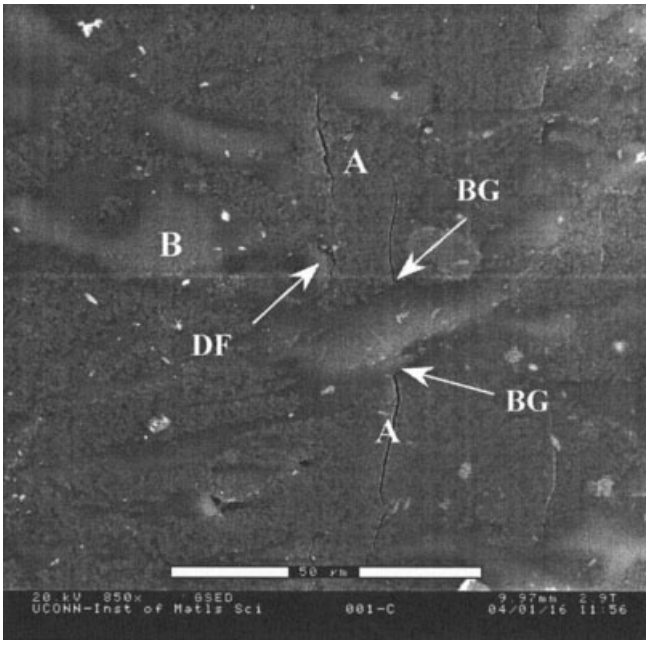

Figure 7 SEM secondary electron image of crack paths in the CNT-filled PET/PVDF blend showing crack bridging (BG) and crack deflection (DF) by the neat PVDF phase. Region A contains CNTs, whereas region B is free from CNTs.[18]

Given that (i) both the CNT-filled PET and the neat polymer phase are self-continuous in 3D space and (ii) the tensile load at the later stage of a tensile test is mainly carried by the bridging ligaments of the neat polymer phase, the tensile stresses at break of the CNT-filled polymer blends can be estimated using the rule of mixtures for composites.[35] Thus, assuming that only the neat polymer phase in the CNT-filled polymer blend carries the load at the point of break, the tensile stress at break for the CNT-filled PET/PVDF blend would be 27 MPa (i.e., 50% of the tensile stress at break for neat PVDF, 54 MPa, because of the presence of about 50 vol % PVDF in the CNT-filled PET/PVDF blend). Similarly, the tensile stress at break would be estimated to be 18 and 15 MPa for the

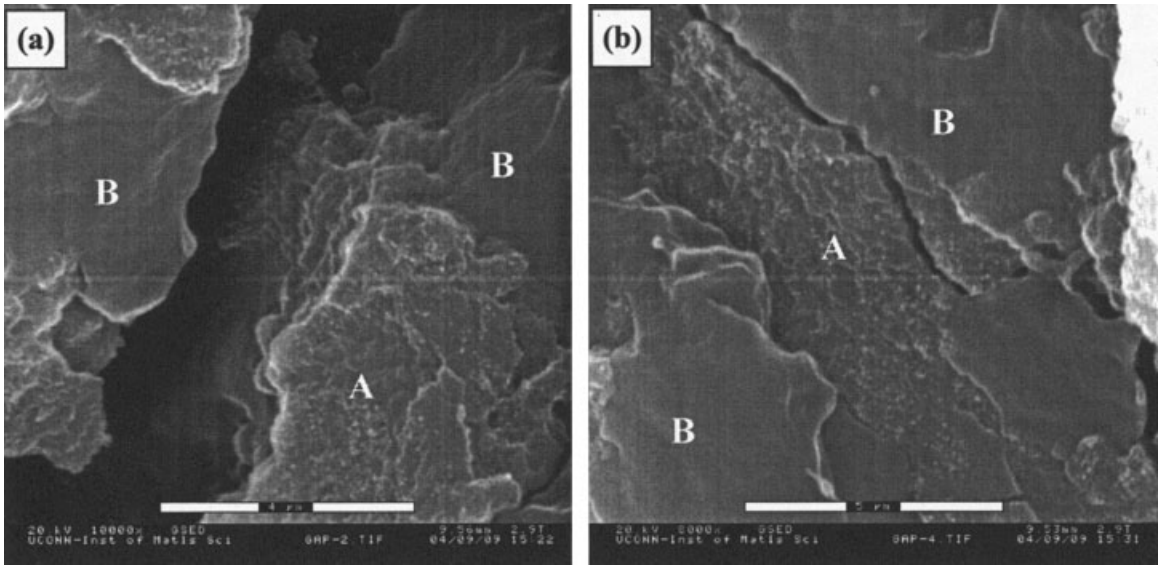

Figure 8 The fracture surface of (a) the CNT-filled PET/PP blend and (b) CNT-filled PET/HDPE blend. The specimens are fractured under tensile loading, and the surfaces shown are perpendicular to the tensile loading axis. Region A contains CNTs, whereas region B is free from CNTs.

CNT-filled PET/PP and CNT-filled PET/HDPE blends, respectively. Comparisons of these estimated tensile stresses at break with the measured values reveal that the measured tensile stress at break for the CNT-filled PET/PVDF blend is about 25% higher than the estimation predicted from the simple rule of mixtures. In contrast, the measured tensile stress at break is about 30% lower than the predicted value for the CNT-filled PET/PP blend, and very close to the prediction for the CNT-filled PET/HDPE blend. The higher tensile stress at break measured from the CNT-filled PET/PVDF than the prediction is presumably related to the constraining effect from the CNT-filled PET region. Such a constraining effect has been observed in ductile metals within the brittle ceramic or intermetallic matrices.[36] Both CNT-filled PET/PP and PET/HDPE blends do not exhibit tensile stresses at break higher than the rule-of-mixtures predictions, which is partially attributed to their relatively large amount of CNT transfer to the neat polymer phase. Such CNT transfer effectively reduces the volume fraction of the neat polymer phase available for carrying the load at the point of break. Thus, from the mechanical property viewpoint it is undesirable to have CNT transfer to the neat polymer phase in the CNT-filled polymer blend.

CONCLUDING REMARKS

The microstructure, mechanical properties, and electrical conductivity of four CNT-filled polymer blend systems have been investigated and analyzed. It can be concluded that the CNT distribution in the polymer blend, which is mainly determined by the wetting coefficient and processing conditions, plays a very important role in both mechanical and electrical properties of all the composites. The preferential location of CNTs in one of the continuous polymer phases in the polymer blend is highly desirable from the viewpoint of the mechanical and electrical properties. Degradations in both mechanical properties and electrical conductivity are observed when some of CNTs transfer to the second polymer phase in the polymer blend. The mechanical properties of the CNT-filled polymer blend are also strongly influenced by the intrinsic properties of the constituent polymers, especially the intrinsic properties of the neat polymer phase. The higher the tensile stress at break for the neat polymer phase in the CNT-filled polymer blend, the better the tensile stress at break for the CNT-filled polymer blend. Processing defects in the CNT-filled polymer blend, such as microcracks, due to the improper injection-molding condition are detrimental to electrical conductivity, as well as mechanical properties, and should be avoided completely.

The authors are indebted to Professors Frano Barbir, Montgomery Shaw, and Lei Zhu for fruitful discussion over a wide range of the topics related to this research. The assistance provided by Dr. Daniel Goberman in argon ion etching, Dr. Tao Zhou and Mr. Hong Luo in tensile tests, and Mr. Juan Villegas in some of SEM observations is greatly appreciated.

References

1. Bar-On, I.; Kirchain, R.; Roth, R. J Power Sources 2002, 109, 71.
2. Besmann, T. M.; Klett, J. W.; Burchell, T. D. Mater Res Soc Symp Proc 1997, 496, 243.

3. Besmann, T. M.; Klett, J. W.; Henry, J. J.; Lara-Curzio, E. J Electrochemical Soc 2000, 147, 4083.
4. Hentall, P. L.; Lakeman, J. B.; Mepsted, G. O.; Adcock, P. L.; Moore, J. M. J Power Sources 1999, 80, 235.
5. Davies, D. P.; Adcock, P. L.; Turpin, M.; Rowen, S. J. J Appl Electrochem 2000, 30, 101.
6. Hornung, R.; Kappelt, G. J Power Sources 1998, 72, 20.
7. Makkus, R. C.; Janssen, A. H. H.; de Bruijn, F. A.; Mallant, R. K. A. M. J Power Sources 2000, 86, 274.
8. Del Rio, C.; Ojeda, M. C.; Acosta, J. L.; Escudero, M. J.; Hontanon, E.; Daza, L. J Appl Polym Sci 2002, 83, 2817.
9. Marsh, G. Materials Today, 2001, 4, 20.
10. Barbir, F.; Braun, J.; Neutzler, J. J New Mater Electrochem Systems 1999, 2, 197.
11. Braun, J.; Zabriskie, J. E., Jr.; Neutzler, J. K.; Fuchs, M.; Gustafson, R. C. U.S. Pat 6,180,275.
12. Miyasaka, K.; Watanabe, K.; Jojima, E.; Aida, H.; Sumita, M.; Ishikawa, K. J Mater Sci 1982, 17, 1610.
13. Grunlan, J. C.; Gerberich, W. W.; Francis, L. F. Polym Eng Sci 2001, 41, 1947.
14. Huang, J.-C. Adv Polym Tech 2002, 21, 299.
15. Xu, C.; Agari, Y.; Matsuo, M. Polym J 1998, 30, 372.
16. Shaw, L. University of Connecticut Invention Disclosure # March 4, 2004, 04.
17. Wu, M.; Shaw, L. Int J Hydrogen Energy 2005, 30, 373.
18. Wu, M.; Shaw, L. J Power Sources 2004, 136, 37.
19. Geuskens, G.; Gielens, J. L.; Geshef, D.; Deltour, R. Eur Polym 1987, 23, 993.
20. Soares, B. G.; Gubbels, F.; Jérôme, R.; Teyssié, P. H. Polym Bull 1995, 35, 223.
21. Soares, B. G.; Gubbels, F.; Jérôme, R.; Vanlanthem, E.; Deltour, R. Chem Technol 1997, 70, 60.
22. Gubbels, F.; Blacher, S.; Vanlanthem, E.; Jérôme, R.; Deltour, R.; Brouers, F.; Teyssié, P. H. Macromolecules 1995, 28, 1559.
23. Tchoudakov, R.; Breuer, O.; Narkis, M.; Siegmann, A. Polym Eng Sci 1996, 36, 1336.
24. Mamunya, Ye. P. J Macromol Sci Phys 1999, B38, 615.
25. Cheah, K.; Simon, G. P.; Forsyth, M. Polym Int 2001, 50, 27.
26. Mallette, J. G.; Márquez, A.; Manero, O.; Castro-Rodríguez, R. Polym Eng Sci 2000, 40, 2272.
27. Foulger, S. H. J Appl Polym Sci 1999, 72, 1573.
28. Feng, J.; Chan, C. M. Polym Eng Sci 1998, 38, 1649.
29. Lee, G. J.; Suh, K. D.; Im, S. S. Polym Eng Sci 2000, 40, 247.
30. Sumita, M.; Sakata, K.; Asai, S.; Miyasaka, K.; Nakagawa, H. Polym Bull 1991, 25, 265.
31. Wu, S. In Polymer Interface and Adhesion; Marcel Dekker: New York, 1982.
32. Technical Data from Goodfellow Corporation Home Page, 2004. Available at http://www.goodfellow.com/csp/active/gfHome.csp.
33. Bueche, F. J Appl Phys 1972, 43, 4837.
34. Wu, G.; Zhang, C.; Miura, T.; Asai, S.; Sumita, M. J Appl Polym Sci 2001, 80, 1063.
35. Agarwal, B. D.; Broutman, L. J. In Analysis and Performance of Fiber Composites, 2nd ed.; Wiley: New York, 1990.
36. Shaw, L.; Abbaschian, R. Metall Trans 1993, 24A, 403.